IEEE Access
Multidisciplinary | Rapid Review | Open Access Journal

Received September 25, 2019, accepted October 26, 2019, date of publication October 29, 2019, date of current version November 8, 2019.

Digital Object Identifier 10.1109/ACCESS.2019.2950346

Multiple-Output ZVS Resonant Inverter Architecture for Flexible Induction Heating Appliances

HÉCTOR SARNAGO, (Senior Member, IEEE), PABLO GUILLÉN, (Student Member, IEEE), JOSÉ M. BURDÍO, (Senior Member, IEEE), AND OSCAR LUCIA, (Senior Member, IEEE)
Electronic Engineering and Communications Department, I3A, Universidad de Zaragoza, 50009 Zaragoza, Spain

Corresponding author: Oscar Lucia (olucia@unizar.es)

This work was supported in part by the Spanish MINECO under Grant TEC2016-78358-R, in part by the Spanish MICINN and AEI under Grant RTC-2017-5965-6, in part by the EU through FEDER program, in part by the DGA-FSE, in part by the MECD under the FPU Grant FPU17/01442, and in part by the BSH Home Appliances Group.

ABSTRACT Flexible cooking surfaces have changed the domestic induction heating product paradigm enabling the use of a wider range of cookware materials, shapes, and positions. In order to implement such systems, multiple-output resonant inverters featuring high-performance and high-efficiency operation while achieving a cost-effective implementation are required. This paper proposes a multiple-output zero-voltage-switching resonant inverter for flexible induction heating appliances. The proposed converter features a matrix structure, enabling a cost-effective implementation with a reduced number of power devices while achieving high performance and low switching losses. It has been tested by means of an experimental prototype featuring 48 induction heating coils, proving the feasibility of the proposed approach.

INDEX TERMS Induction heating, home appliances, resonant power conversion, inverters.

I. INTRODUCTION

Induction heating technology has evolved since its industrial origins to enable a wide range of industrial, domestic and biomedical applications [1]. Advances in key enabling technologies, such as power electronic devices and topologies, digital control and magnetic components have enabled the development of high performance and high efficiency systems outperforming other classical heating technologies.

Among the existing applications, domestic induction heating [2]–[4] has remarkably become a leading technology in this category in the last decade [5]. These systems exhibit faster heating, higher performance and efficiency, more accurate control, and safer operation. In this context, modern design trends are focused towards flexible IH appliances (Fig. 1) [6]–[8], aiming to the highest level of flexibility and user performance yet to come. In order to design and implement such systems, a special effort must be made on the design of multi-coil power electronics architectures achieving both high performance and cost-effective implementations.

The associate editor coordinating the review of this manuscript and approving it for publication was Yang Han.

FIGURE 1. Flexible IH appliance.

In the last decade, several power converters have been proposed, all of them having in common the search of an optimum balance between cost, performance, and control complexity. These converters can be classified according to the base architecture from which they are derived, as it is shown in Fig. 2.

The most straight-forward approach is based on using a power converter to supply each coil (Fig. 2.(a)). To achieve a cost-effective solution, typically single-switch class-e inverters [9] have been studied and proposed as a feasible

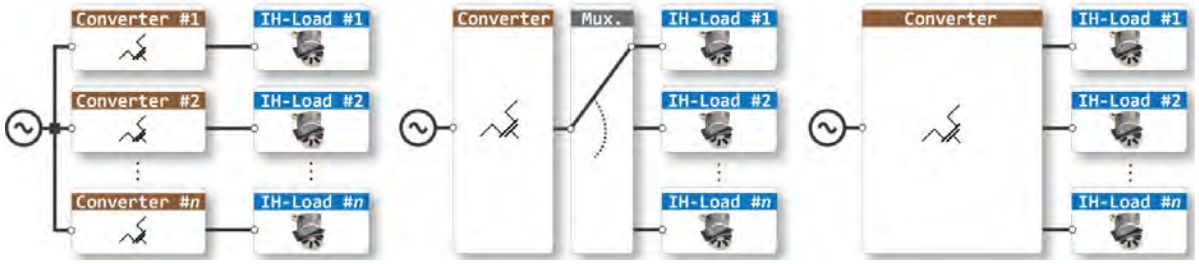

FIGURE 2. Flexible IH appliance implementations.

implementation which only requires one power device per inductor [10]. However, when implementing flexible domestic induction appliances with a high number of coils, this approach suffers from severe control constraints due to intermodulation acoustic noise, power restrictions, and degraded soft-switching operation. As a consequence, this approach is usually limited to low power and low inductor number implementations.

The second approach (Fig. 2.(b)) is based on using a single main inverter which is connected through a multiplexing network to the coils [11], [12]. This approach is the most common nowadays in the market and typically uses an electromechanic relay network to configure the inverter output according to the user requirement. While being a cost-effective solution, this approach has severe limitations due to the use of relays such as the noise [13], [14] or limited switching times, and usually requires of complex IH load identification systems [15]–[17] to ensure proper converter operation.

Finally, the third approach is based on using a multiple-output resonant converter to supply several coils simultaneously (Fig. 2.(c)). This approach offers a higher performance and, consequently, has been the target of many researchers in the past years. In [18], a half-bridge for high-power concentric-inductor domestic IH is proposed. Considering a higher number of coils, [11], [19] proposes a three-device half-bridge structure that achieves a significant cost reduction [20] focuses on multi-load control, using an intermediate dc-dc converter to provide higher versatility. A different approach is proposed in [21], where different resonant frequencies are set at each coil to perform frequency selection. Finally, in [22]–[24], the series resonant multi-inverter is proposed as a topology with reduced number of switching devices and versatile control, which is extended to ac-ac operation in [25]. When higher output power is required, the third family of topologies derived from the full-bridge converter are preferred. In [26]–[29], the association of multiple full-bridge topologies is proposed to implement a multi-inductor structure, and in [30] the use of a multiple-output full bridge converter is proposed to enable a cost-effective high-power implementation.

This paper is focused on the development of a high-performance and cost-effective multiple output resonant converter for multi-coil IH appliances. The previously reviewed implementations are derived from single-output converters and, consequently, have inherent limitations when used as multiple-output converters. In the past, a matrix zero current switching (ZCS) converter [31] has been proposed. However, the output power control is severely constrained by frequency restrictions to avoid acoustic noise, being necessary the use of bust-mode operation. In this paper, a zero-voltage-switching (ZVS) resonant matrix converter is proposed for multi-coil induction heating appliances. The proposed converter achieves a reduced number of power devices while ensuring high efficiency and proper power control in each coil. Unlike previous proposals, the proposed converter enables full output power control, ensuring the highest level of user performance and flexibility in any domestic induction heating appliances.

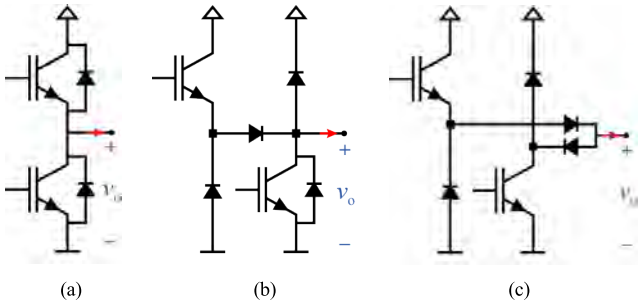

FIGURE 3. Splitted inverter branch derivation: (a) half-bridge inverter, (b) semi-split output inverter, and (c) split-output inverter.

The remainder of this paper is organized as follows. Section II introduces the proposed ZVS multiple output resonant converter topology. Section III analyzes the converter operation including its main states, waveforms and expressions determining its operation, as well as the main modulation strategies. Section IV explains the main implementation and experimental results, detailing an innovative implementation and the main waveforms obtained. Finally, Section V draws the main conclusions of this paper.

II. ZVS MULTIPLE-OUTPUT RESONANT CONVERTER

A. PROPOSED TOPOLOGY DERIVATION

To achieve a high-performance and cost-effective implementation, a ZVS resonant matrix converter is proposed.

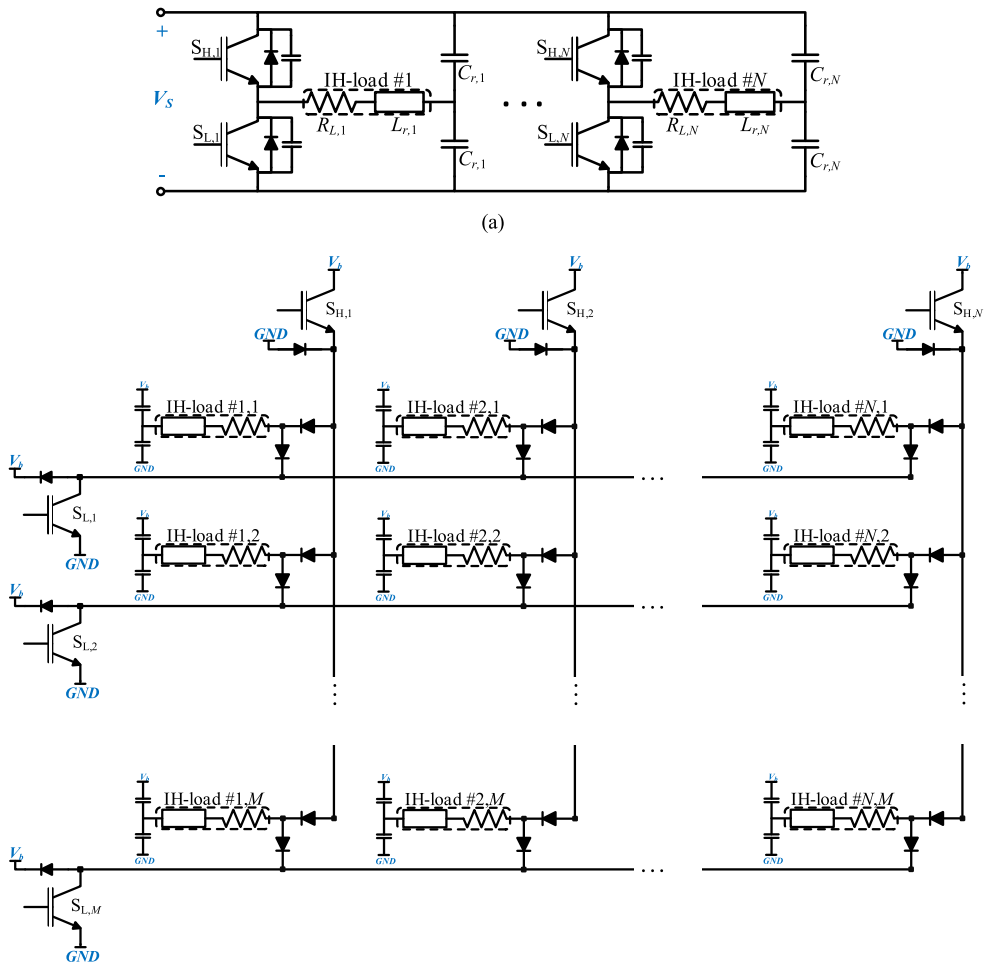

FIGURE 4. Multiple output implementations: (a) redundant half-bridge implementation, (b) multiple-Output resonant ZVS matrix converter.

The basic building block to implement a ZVS inverter is the half-bridge configuration (Fig. 3(a)), which uses IGBTs with antiparallel diodes. From this configuration, the semi-split output half-bridge inverter is derived, Fig. 3(b), where an anti-parallel diode is replaced by a series configuration, making possible to build a cascaded arrangement of low-side devices. Finally, Fig. 3 (c) shows the split-output inverter configuration, which is usually used to improve the dynamic performance of the converter with reduced device number. This will be building block used to construct the proposed multiple-output topology with significant advantage over the previously discussed state-of-the-art converters.

Considering the series-resonant half-bridge inverter, a feasible implementation to achieve a multi-coil implementation sharing a common bus voltage Vs is shown in Fig. 4 (a). However, it is clear that this topology requires a high number of power devices and it is not suitable for flexible IH appliances. To overcome this limitation, the multiple-output resonant ZVS matrix converter is proposed (Fig. 4 (b)).

The proposed converter follows a matrix structure, where the main power devices are placed in a column and row, and each IH load occupies a position in the matrix. Each column/row switch is implemented using a combination of transistor $S_{H,i}$, $S_{L,i}$ and diode. Besides, IH loads are connected through a pair of diodes to block voltage. Each induction heating load (i, j) is modelled by the series connection of an inductor $L_{r,(i,j)}$ and a resistor $R_{L,(i,j)}$. Besides, the resonant capacitor $C_{r,(i,j)}$ is split to improve input current consumption. Note that each resonant tank Lr-C_r-$R_{L(i,j)}$ is different, depending on the IH load placed by the user and being affected by a wide number of factors: material, geometry, coupling, or temperature, among others.

The proposed topology achieves the maximum output power at the resonant frequency and increases it to reduce the power, operating consequently with inductive load and ZVS operating conditions. This enables to avoid the acoustic noise as well as achieving soft-switching turn-on conditions.

One of the main advantages of the proposed topology is that it achieves a significant reduction in the number of

required power devices. This enables a cost reduction, not only due to the power devices, but also due to the driving and protection circuits, PCB, and improved MTBF. For instance, a typical 48-coil flexible IH appliance would reduce the required number of devices from $2n = 96$ with an n half-bridge implementation, to $2 \cdot ceil(\sqrt{n}) = 14$ by using the proposed ZVS matrix topology. Also, and considering a smart coil distribution, this topology makes possible to design a maximum P_o output power at each coil while minimizing the maximum appliance power consumption and, therefore, power device ratings. This is usually a significant advantage because although the power per coil can be 600 W for a 48-coil implementation, the maximum appliance power is limited by regulations and/or user constrains to 3600/7200 W. Also, together with the component reduction power density is also greatly improved, allowing for built-in implementations, which are mandatory for most houses' installations.

The second advantage is derived from the full-silicon implementation and its modulation strategies. The proposed topology achieves independent output-power control in the complete operating range individually for each load. Besides, each coil can be used as pot detection system by activating individually the desired coil. Consequently, by measuring the current/voltage in each coil, it is possible to identify the ones coupled with the target pot. This contrasts with those low-cost implementations using EM relays, which also suffer from acoustic noise, and provides a new standard of performance powering new potential advantages for the user.

In conclusion, the proposed topology presents significant advantages from the power electronics, control and implementation points of view, providing important benefits to improve the user performance in advanced IH products. Next sections present a detailed analysis of the topology and its design and experimental verification, and efficiency results are discussed and compared in the experimental results section.

III. ANALYSIS OF THE PROPOSED CONVERTER

A. CONVERTER OPERATION

The proposed converter exhibits an operation corresponding to a half-bridge series resonant converter [32]. When each individual cell (i, j) is activated, the converter operation for the corresponding column switch (sub-index H) and row switch (sub-index L) is as described in Fig. 5. When the current is positive, the current flows firstly through the S_H transistor, which is activated under ZVS conditions. Once S_H is deactivated, the current flows through D_L (State II) until the current becomes negative due to the resonant behavior. The negative current flows then through S_L (State III) until this switch is deactivated and the current flows through D_H (State IV). Moreover, all the transistors operate under ZVS conditions during the turn-on transition, leading to a high-efficiency operation.

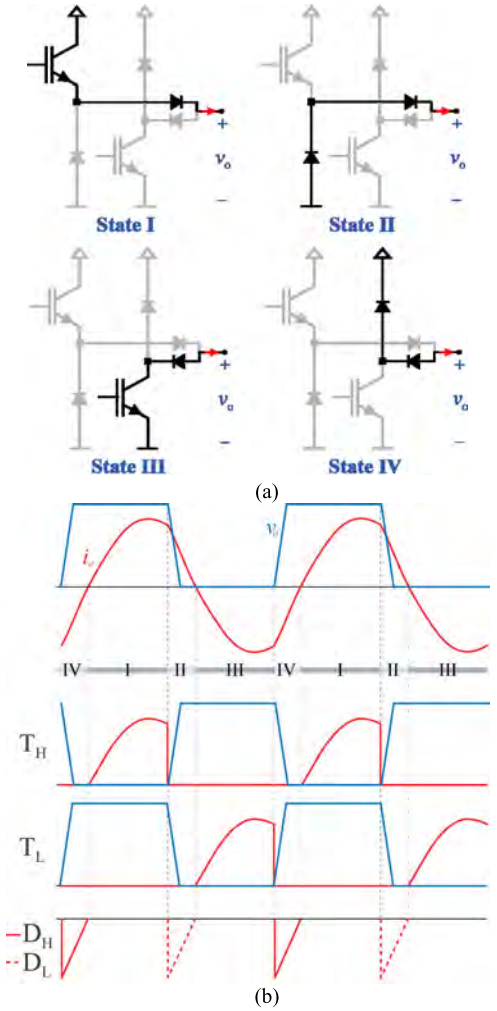

FIGURE 5. Proposed matrix ZVS resonant inverter topology equivalent states (a) and main waveforms through transistors T and diodes D (b).

The proposed converter operates under ZVS conditions provided that it is operated above the resonant frequency and, consequently, transistor turn-on losses during transitions IV-I and II-III, respectively, can be neglected. Moreover, diodes operate only with turn-on losses, which can be also usually neglected. Therefore, the main power loss sources are conduction losses and turn-off losses. Considering the output power/current ranges, and the switching frequency ranges, typically between 20 kHz, to avoid acoustic noise, and 100 kHz, IGBT technology is proposed as the best cost-performance solution.

The operation of the proposed power converter can be described as a function of the state variable in each IH load, i.e. inductor current and resonant capacitor voltage. By performing Fourier analysis, the resonant capacitor voltage in each IH load $v_{c,(i,j)}(t)$ can be expressed as

$$v_{c,(i,j)}(t) = \sum_{h=0}^{H} \left(A_{h,(i,j)} \cos(h\omega_s t) + B_{h,(i,j)} \sin(h\omega_s t) \right), \quad (1)$$

and, consequently, the output current for each IH load $i_{o,(i,j)}(t)$ is derived as follows

$$i_{o,(i,j)}(t) = \omega_s C_{r,(i,j)} \sum_{h=1}^{H} \left(B_{h,(i,j)} h \cos(h\omega_s t) - A_{h,(i,j)} h \sin(h\omega_s t) \right). \quad (2)$$

Note that the current in each column (S_H) and row (S_L) device will be the sum of the current through the active loads in each column and row, respectively, and that in a standard operation, the switching frequency, ω_s, and duty cycle, D, will be considered the same for all IH loads at this point.

Since the operation of each IH load is independent, the output power in each load $P_{o,(i,j)}$ can be calculated by the following integral expression:

$$P_{o,(i,j)} = \frac{1}{T_{sw}} \int_0^{T_{sw}} v_{o,(i,j)}(t - t_0) \cdot i_{o,(i,j)}(t) dt, \quad (3)$$

where the output voltage is expressed as a function of the switching device states as follows

$$v_{o,(i,j)}(t) = \begin{cases} V_s & (0 \leq t \leq DT_{sw}) \\ 0 & (DT_{sw} < t \leq T_{sw}). \end{cases} \quad (4)$$

By combining the previous expressions, the output power can be expressed as a function of the Fourier coefficients and operation conditions, i.e. switching frequency and duty cycle,

$$P_{o,(i,j)} = \frac{A_{0,(i,j)}}{DT_{sw}} C_{r,(i,j)} \sum_{h=0}^{H} \left(A_{h,(i,j)} \left[\cos(h2\pi D) - \cos(h\omega_s t_0) \right] + B_{h,(i,j)} \left[\sin(h2\pi D) - \sin(h\omega_s t_0) \right] \right). \quad (5)$$

Finally, by assuming square waveform modulation, i.e. symmetrical modulation with $D = 0.5$, the output power expression can be simplified to

$$P_{o,(i,j)} = -4A_{0,(i,j)} f_{sw} C_{r,(i,j)} \sum_{h=1,h\text{odd}}^{H} A_{h,(i,j)}, \quad (6)$$

and the total output power is calculated as the sum of the individual IH coil terms $P_o = \sum_{i,j} P_{o,(i,j)}$, where the Fourier coefficients for the considered waveforms are

$$A_{h,(i,j)} = -\frac{2V_s R_{L,(i,j)}}{h^2 \pi \omega_s C_{r,(i,j)} \left(R_{L,(i,j)}^2 + \left(\omega_s h L_{r,(i,j)} - \frac{1}{\omega_s h C_{r,(i,j)}} \right)^2 \right)}, \quad (7)$$

$$B_{h,(i,j)} = -\frac{2V_s \left(\omega_s h L_{r,(i,j)} - \frac{1}{\omega_s h C_{r,(i,j)}} \right)}{h^2 \pi \omega_s C_{r,(i,j)} \left(R_{L,(i,j)}^2 + \left(\omega_s h L_{R,(i,j)} - \frac{1}{\omega_s h C_{r,(i,j)}} \right)^2 \right)}. \quad (8)$$

TABLE 1. Main test-bench parameters.

Parameter	Value
Power per load	600 W
Total power	2 x 3600 W
Switching frequency range	[20 - 100] kHz
Power devices	IGBT IKD15N60RF
Resonant tank	15 Ω, 150 µH, 44 nF
Control device	FPGA Xilinx S6 XC6SLX45

IV. IMPLEMENTATION AND EXPERIMENTAL RESULTS

A. EXPERIMENTAL PROTOTYPE

In order to test and prove the feasibility of the proposed topology, a domestic induction heating prototype has been designed and implemented. The experimental test-bench has been designed to implement a high-end domestic induction heating appliance featuring a 48-coil configuration. Each coil has a rated maximum power of 600 W, being 3600 W the maximum simultaneous power consumption to fulfill EMC standards. Table 1 summarizes the main test-bench parameters.

The design methodology for this converter is similar to other domestic induction heating systems [22], [32]. The resonant tank is designed to obtain, at least, the required maximum power with 230 V rms input voltage, so R_L is defined. After that, and for a given geometry, 8-cm coils for this flexible implementation, the values of the equivalent inductance are given L_r. Finally, the resonant capacitor is set to obtain a resonant frequency above the audible range, typically above 20 kHz.

Due to the high power-density requirements and the limited cooling possibilities, the prototype thermal performance is a key design challenge. In order to take the most of the available volume and form factor of an IH appliance, a design based on an insulated metal substrate has been proposed (Fig. 6). The proposed implementation takes advantage of the distributed power device implementation and the surface availability, and it combines IMS technology for power devices and standard FR4 PCB for control and auxiliary circuits. By doing so, a proper thermal management can be ensured, and a cost-effective implementation is achieved thanks to advances and widespread utilization of IMS technology. Fig. 6 shows a detailed view of the IMS PCB for power devices (a), the control and auxiliary circuit board (b), including the mains rectifier, and the complete assembled unit (c). In the last figure, the IMS board containing the power devices is seen from the bottom layer to be attached to a heatsink.

Finally, in order to ensure the proper thermal performance, FEM simulation using COMSOL® software has been performed. Fig. 7 shows the simulation results for a worst-case operation consisting on 6 loads activated with maximum output power, i.e. 3600 W, and located in the same area. As it can be seen, IMS ensures proper thermal dissipation

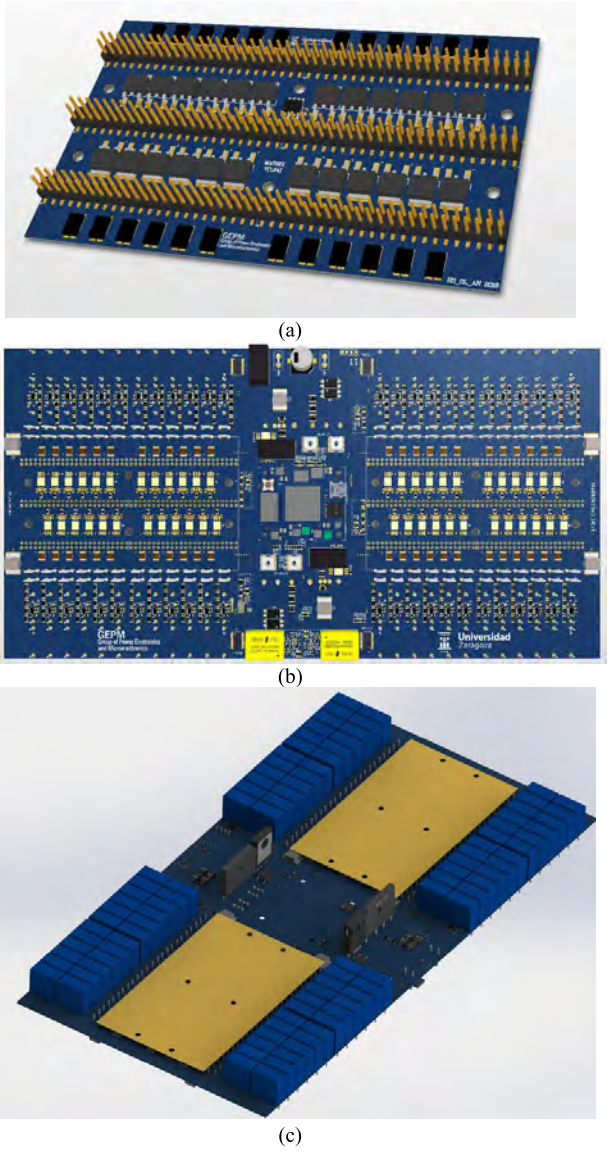

FIGURE 6. Experimental prototype 3D render: (a) IMS power board, (b) control and resonant capacitor board, and (c) complete assembly.

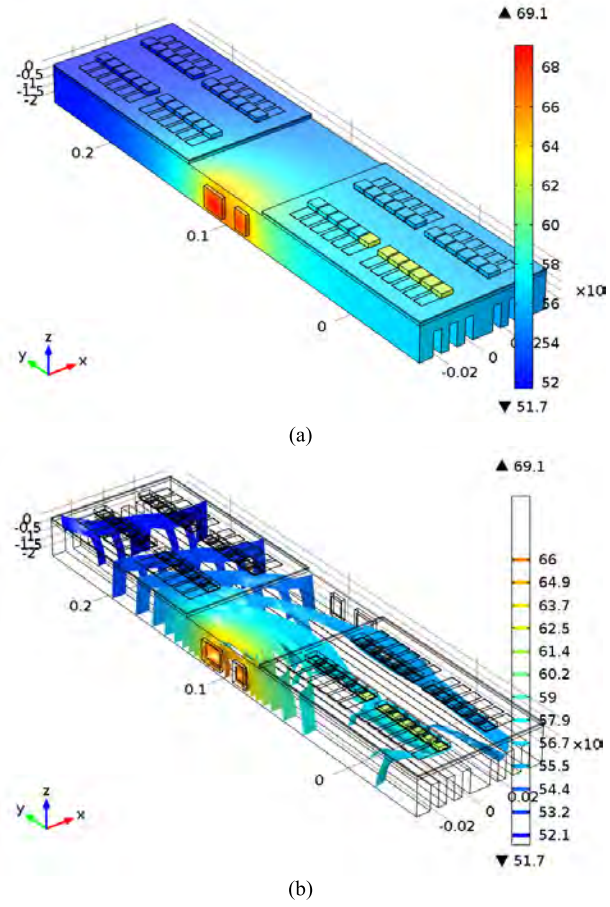

FIGURE 7. Thermal simulation (temperature maps, units °C): temperature field (a) and temperature isosurfaces (b) for 3600 W operation.

to the ambient, achieving an operating temperature lower than 64 °C for IMS devices. The highest temperature is estimated to be at the input rectifier stage, allocated in the lateral of the heat-sink. Assuming 25 °C ambient temperature, the maximum temperature achieved is below 70 °C, being this design coherent with other commercial designs and proving the feasibility of this proposal.

B. CONTROL ARCHITECTURE

The control architecture is designed to monitor and control all the coils present in the proposed topology. To perform this tsk while ensuring a cost-effective implementation, each IH cell has been designed as shown in Fig. 9.

The resonant capacitor has been placed following a split structure in order to improve bus current consumption. In the proposed implementation, the resonant capacitor voltage is measured. This enables a cheap and efficient method to estimate the main required parameters, including the output power and the estimated quality factor, required to identify the IH load coupling quality [33].

This information is used by the FPGA-based control architecture to preform three tasks. Firstly, variations in resonant capacitor voltage enables calculating the output power avoiding the need of expensive current sensors. Consequently, unlike multiplexed approaches, the output power can be controlled individually at each coil, providing improved heat distribution and avoiding problems of excessive current in partially coupled loads. This task is performed using a standard PI controller, since the dynamics of the power converter are several orders of magnitude faster than the thermal system. Secondly, this information is used to monitor ZVS conditions. As a consequence, the correct and efficient operation of the inverter can be controlled, ensuring improved efficiency and reliability. Finally, this system enables to perform a real-time pot detection system (PDS). This enables to detect the coils covered prior to the heating process, as well as to track in real time any movement to prevent sudden changes in the resonant tank.

(a) (b)

FIGURE 8. Experimental prototype: (a) IMS power board and (b) control and resonant capacitor board.

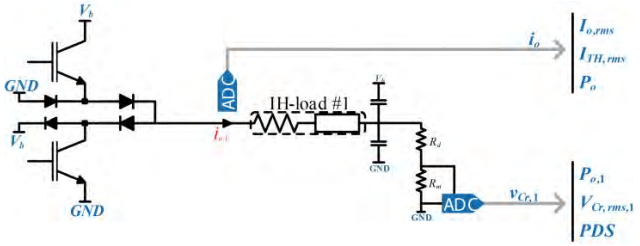

FIGURE 9. Measurement and IH load identification system.

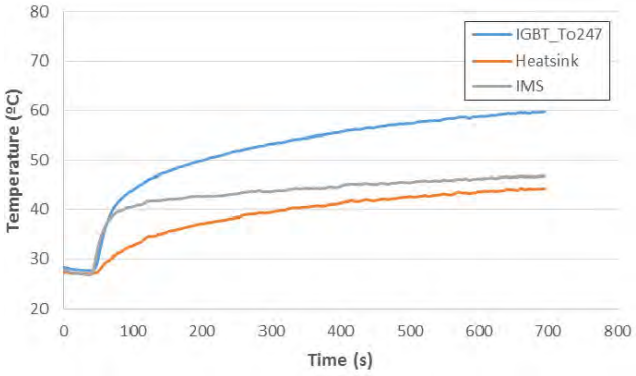

FIGURE 10. Experimental prototype thermal evolution at maximum output power (3600 W): temperature in main IGBT, heatsink and IMS power board.

The proposed control architecture is implemented using FPGA technology to take advantage of its parallel processing, enabling the real-time control of the whole system. The final target is an ASIC-based control to obtain a cost-effective implementation for the domestic induction heating market.

C. EXPERIMENTAL RESULTS

The designed prototype has been implemented and tested to analyze its performance and prove the feasibility of this proposal. Fig. 8 shows a detailed view of the complete prototype, consisting on 2 IMS power boards containing the power transistors and diodes (Fig. 8 (a)), and a common control board containing an FPGA-based control architecture, driving circuits and resonant capacitors (Fig. 8 (b)).

Fig. 10 (a) shows the main waveforms of the proposed converter, including the input voltage and current, output voltage and current, and one control signal for one specific coil. From this figure, it can be seen that the converter operates as expected, and that ZVS is achieved during the turn-on transition in the power devices. This test is performed using 6 active coils, yielding 3600 W input power and 16.37 A input RMS current, respectively. Once the correct converter operation is confirmed at maximum output power, Fig. 10(b) shows a detailed operation of different coils with different output power. The output power is controlled by using high-frequency pulse density modulation, so the power can be individually controlled in each load.

In order to prove the proper thermal performance, experimental studies operating at maximum power have been performed. Since the nature of the application makes difficult the use of standard thermography, 3 thermocouples have been placed in the most relevant points, i.e., the heatsink, TO-247 component in the lateral of the heatsink, and the IMS board. The temporal evolution of the temperature for maximum output power is shown in Fig. 11. As it can be seen, the proposed converter can operate for more than

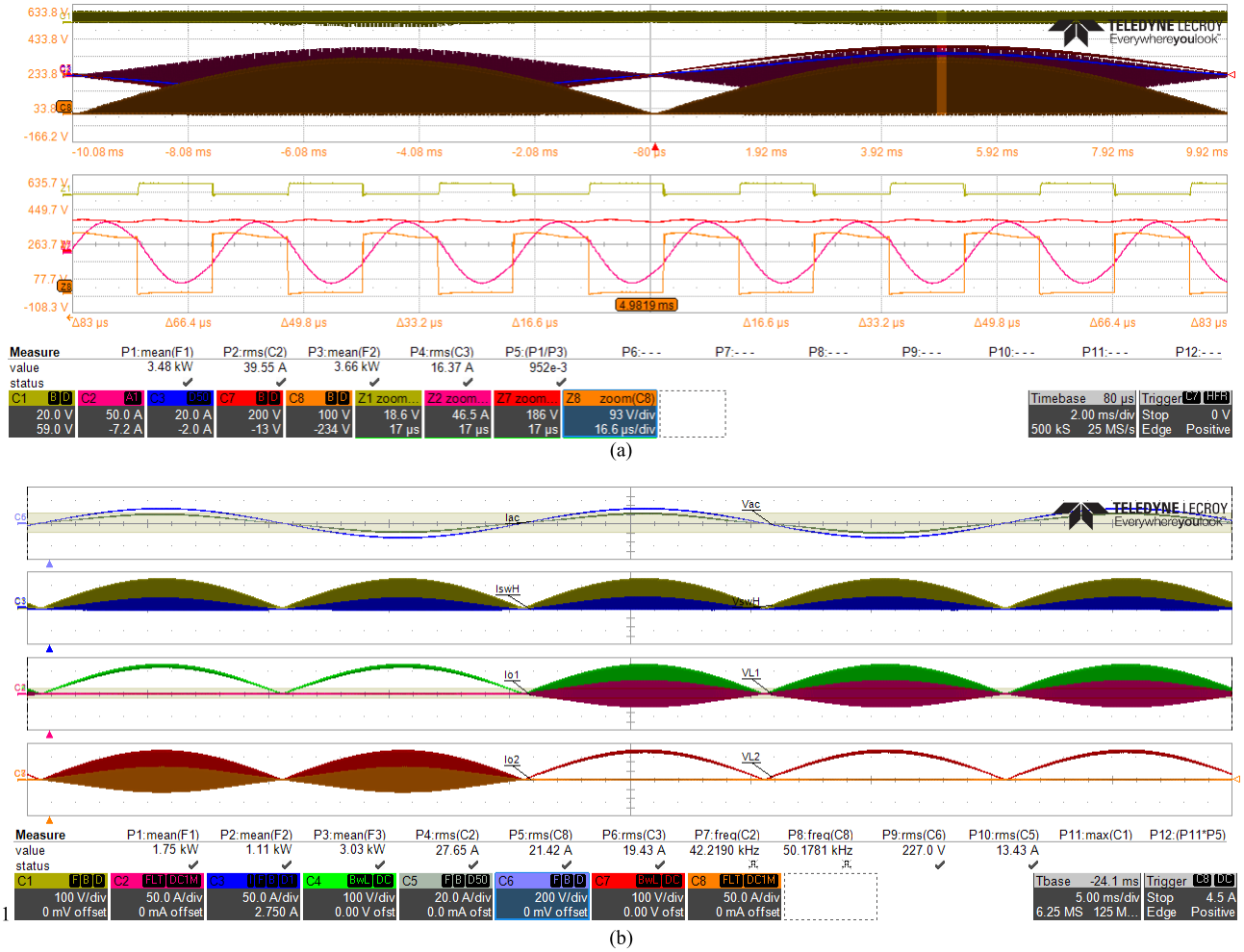

FIGURE 11. **Main waveforms of the proposed converter: input voltage and current, and output voltage and current. (a) 6 active coils operating at maximum power, 3600 W, and (b) 6 active coils (2 represented) operating with pulse density modulation.**

10 minutes at maximum power without exceeding a temperature increment higher than 30 °C. These results improve significantly current technology and enable continuous operation at maximum power for longer cooking times without power deratings.

Aligned with this analysis, the efficiency of the proposed power converter has been measured under different configurations of output power and active coils, which represents different cooking configurations with different cookware (Fig. 12). In this figure, it can be seen that the achieved efficiency is above 96% in all the operating range. In order to avoid low efficiency at very low output power levels, PDM modulation is applied to avoid higher switching frequencies. Moreover, medium-power operation, which is the most common for domestic IH appliances, achieve efficiencies above 97%, being a remarkable achievement for IH power converters featuring cost-effective silicon devices.

Finally, unlike previous proposals, one of the main benefits of the proposed converter is the ability to detect using the power converter the presence of an induction heating load. To illustrate this feature, Fig. 13 shows the main waveforms obtained when no-load is present (a) and a standard ferromagnetic pot is present (b). From this figure, it is clear that the change in the current shape and consumed power are evident. Since these parameters are being measured with the proposed control architecture, this makes possible to detect and selectively activate only those coils that have a proper electromagnetic coupling with an IH load. This contrast with current state-of-the-art implementations where several coils are shared by a common inverter, making impossible individual detection and adapting the operating conditions.

As a conclusion of the experimental design and analysis, the proposed topology has performed as expected from an operative, thermal, and efficiency points of view. Consequently, the proposed topology is proved to be a high-performance and cost-effective implementation for future flexible induction heating appliances.

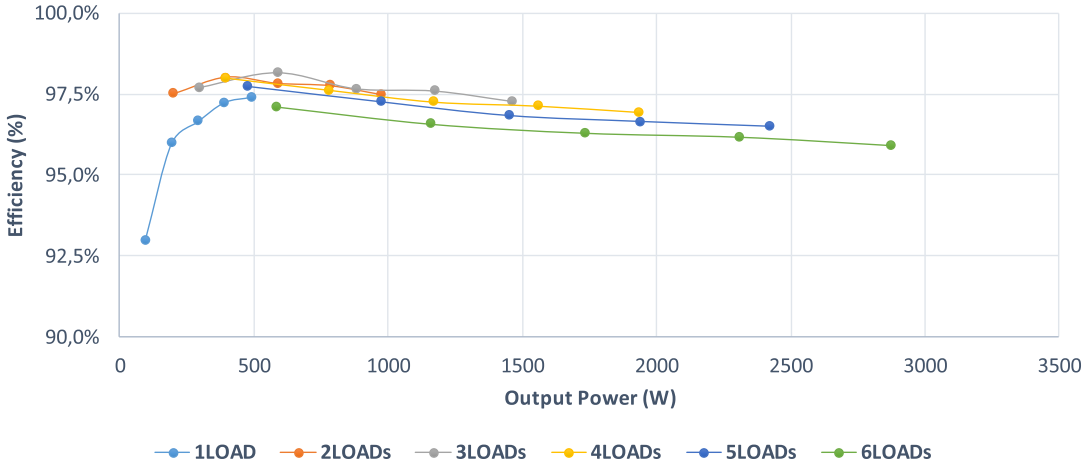

FIGURE 12. Experimental efficiency with continuous modulation for different combinations of loads and output powers.

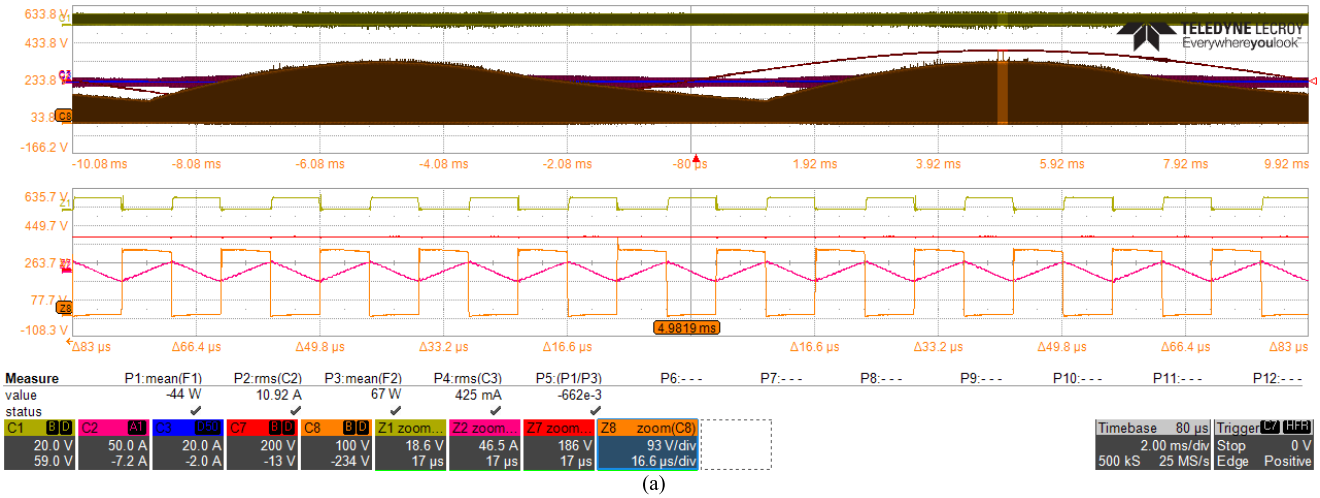

(a)

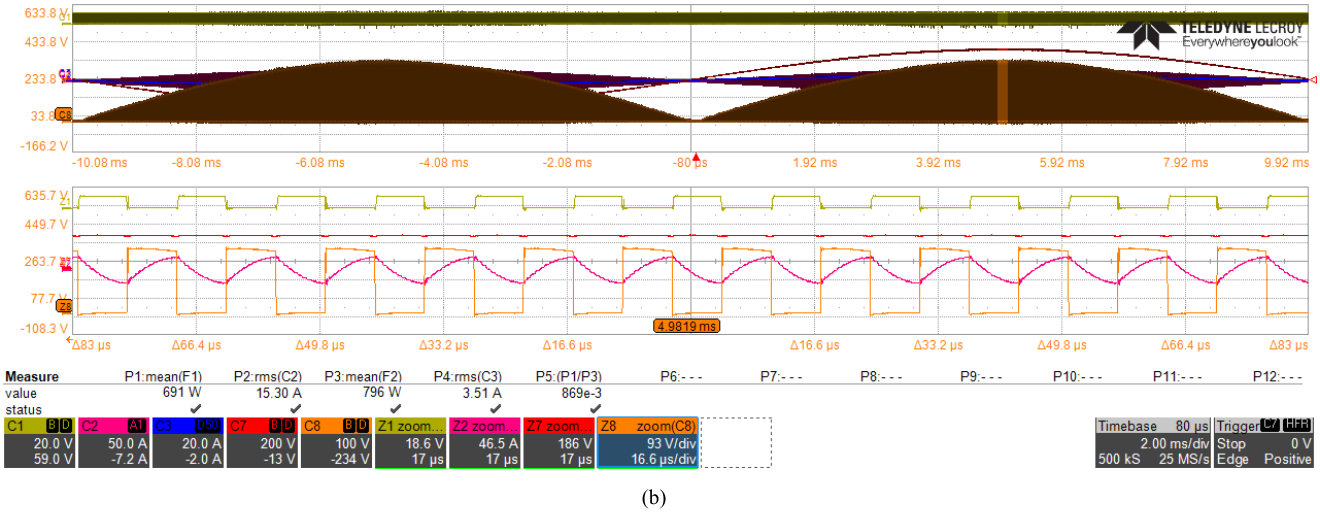

(b)

FIGURE 13. Proposed converter waveforms with no-load (a) and with standard ferromagnetic IH load (b). From top to bottom: control signal, output voltage, mains voltage, and output current (zoom in the lower part of the picture).

V. CONCLUSION

This paper has proposed a multiple-output ZVS resonant inverter featuring a matrix structure that enables a significant power device reduction. The proposed topology enables full power control and IH load detection at each coil, improving significantly the performance of the power converter.

Moreover, the high-efficiency ZVS operation together with an improved thermal design taking advantage of IMS technology makes possible to achieve a higher performance level.

The proposed topology has been designed and implemented in a 48-coils full-flexible IH appliance. The experimental results, including waveforms, thermal performance and efficiency prove the feasibility of this proposal. As a conclusion, the presented topology is proposed to be a high-performance and cost-effective power converter to push forward flexibility and user-performance in modern induction heating appliances.

REFERENCES

[1] Ó. Lucía, P. Maussion, E. J. Dede, and J. M. Burdío, "Induction heating technology and its applications: Past developments, current technology, and future challenges," *IEEE Trans. Ind. Electron.*, vol. 61, no. 5, pp. 2509–2520, May 2014.

[2] W. Han, K. T. Chau, C. Jiang, and W. Liu, "All-metal domestic induction heating using single-frequency double-layer coils," *IEEE Trans. Magn.*, vol. 54, no. 11, Nov. 2018, Art. no. 8400705.

[3] H.-P. Park and J.-H. Jung, "Load-adaptive modulation of a series-resonant inverter for all-metal induction heating applications," *IEEE Trans. Ind. Electron.*, vol. 65, no. 9, pp. 6983–6993, Sep. 2018.

[4] S. Komeda and H. Fujita, "A phase-shift-controlled direct AC-to-AC converter for induction heaters," *IEEE Trans. Power Electron.*, vol. 33, no. 5, pp. 4115–4124, May 2018.

[5] T. Mai, D. Steinberg, J. Logan, D. Bielen, K. Eurek, and C. McMillan, "An electrified future: Initial scenarios and future research for U.S. energy and electricity systems," *IEEE Power Energy Mag.*, vol. 16, no. 4, pp. 34–47, Jul./Aug. 2018.

[6] Ó. Lucía, J. Acero, C. Carretero, and J. M. Burdío, "Induction heating appliances: Toward more flexible cooking surfaces," *IEEE Ind. Electron. Mag.*, vol. 7, no. 3, pp. 35–47, Sep. 2013.

[7] W. Han, K. T. Chau, Z. Zhang, and C. Jiang, "Single-source multiple-coil homogeneous induction heating," *IEEE Trans. Magn.*, vol. 53, no. 11, Nov. 2017, Art. no. 7207706.

[8] V. T. Kilic, E. Unal, N. Yilmaz, and H. V. Demir, "All-surface induction heating with high efficiency and space invariance enabled by arraying squircle coils in square lattice," *IEEE Trans. Consum. Electron.*, vol. 64, no. 3, pp. 339–347, Aug. 2018.

[9] A. K. Lefedjiev and L. Hobson, "Single ended resonant power supply for induction heating," *Electron. Lett.*, vol. 26, no. 12, pp. 814–816, Jun. 1990.

[10] H. Sarnago, Ó. Lucía, A. Mediano, and J. M. Burdío, "A class-E direct AC–AC converter with multicycle modulation for induction heating systems," *IEEE Trans. Ind. Electron.*, vol. 61, no. 5, pp. 2521–2530, May 2014.

[11] F. Forest, S. Faucher, J.-Y. Gaspard, D. Montloup, J.-J. Huselstein, and C. Joubert, "Frequency-synchronized resonant converters for the supply of multiwinding coils in induction cooking appliances," *IEEE Trans. Ind. Electron.*, vol. 54, no. 1, pp. 441–452, Feb. 2007.

[12] M. Fernández, X. Perpiñà, J. Rebollo, M. Vellvehi, D. Sánchez, T. Cabeza, S. Llorente, and X. Jordà, "Solid-state relay solutions for induction cooking applications based on advanced power semiconductor devices," *IEEE Trans. Ind. Electron.*, vol. 66, no. 3, pp. 1832–1841, Mar. 2019.

[13] E. Ramirez-Laboreo, C. Sagues, and S. Llorente, "A new run-to-run approach for reducing contact bounce in electromagnetic switches," *IEEE Trans. Ind. Electron.*, vol. 64, no. 1, pp. 535–543, Jan. 2017.

[14] E. Ramirez-Laboreo, E. Moya-Lasheras, and C. Sagues, "Real-time electromagnetic estimation for reluctance actuators," *IEEE Trans. Ind. Electron.*, vol. 66, no. 3, pp. 1952–1961, Mar. 2019.

[15] H. Sarnago, Ó. Lucía, and J. M. Burdío, "FPGA-based resonant load identification technique for flexible induction heating appliances," *IEEE Trans. Ind. Electron.*, vol. 65, no. 12, pp. 9421–9428, Dec. 2018.

[16] H. Sarnago, O. Lucia, D. Navarro, and J. M. Burdío, "Operating conditions monitoring for high power density and cost-effective resonant power converters," *IEEE Trans. Power Electron.*, vol. 31, no. 1, pp. 488–496, Jan. 2016.

[17] O. Jiménez, Ó. Lucía, I. Urriza, L. A. Barragan, D. Navarro, and V. Dinavahi, "Implementation of an FPGA-based online hardware-in-the-loop emulator using high-level synthesis tools for resonant power converters applied to induction heating appliances," *IEEE Trans. Ind. Electron.*, vol. 62, no. 4, pp. 2206–2214, Apr. 2015.

[18] I. Millán, J. M. Burdío, J. Acero, Ó. Lucía, and D. Palacios, "Resonant inverter topologies for three concentric planar windings applied to domestic induction heating," *Electron. Lett.*, vol. 46, no. 17, pp. 1225–1226, Aug. 2010.

[19] Y.-C. Jung, "Dual half bridge series resonant inverter for induction heating appliance with two loads," *Electron. Lett.*, vol. 35, no. 16, pp. 1345–1346, Aug. 1999.

[20] H. P. Ngoc, H. Fujita, K. Ozaki, and N. Uchida, "Phase angle control of high-frequency resonant currents in a multiple inverter system for zone-control induction heating," *IEEE Trans. Power Electron.*, vol. 26, no. 11, pp. 3357–3366, Nov. 2011.

[21] F. Forest, E. Laboure, F. Costa, and J. Y. Gaspard, "Principle of a multi-load/single converter system for low power induction heating," *IEEE Trans. Power Electron.*, vol. 15, no. 2, pp. 223–230, Mar. 2000.

[22] Ó. Lucía, J. M. Burdío, L. A. Barragán, J. Acero, and I. Millán, "Series-resonant multiinverter for multiple induction heaters," *IEEE Trans. Power Electron.*, vol. 25, no. 11, pp. 2860–2868, Nov. 2010.

[23] Ó. Lucía, J. M. Burdío, L. A. Barragán, C. Carretero, and J. Acero, "Series resonant multiinverter with discontinuous-mode control for improved light-load operation," *IEEE Trans. Ind. Electron.*, vol. 58, no. 11, pp. 5163–5171, Nov. 2011.

[24] Ó. Lucía, H. Sarnago, and J. M. Burdío, "Soft-stop optimal trajectory control for improved performance of the series-resonant multiinverter for domestic induction heating applications," *IEEE Trans. Ind. Electron.*, vol. 62, no. 10, pp. 6251–6259, Oct. 2015.

[25] Ó. Lucía, C. Carretero, J. M. Burdío, J. Acero, and F. Almazan, "Multiple-output resonant matrix converter for multiple induction heaters," *IEEE Trans. Ind. Appl.*, vol. 48, no. 4, pp. 1387–1396, Jul. 2012.

[26] H. Pham, H. Fujita, K. Ozaki, and N. Uchida, "Dynamic analysis and control of a zone-control induction heating system," in *Proc. IEEE Energy Convers. Congr. Expo. (ECCE)*, Sep. 2011, pp. 4093–4100.

[27] H. N. Pham, H. Fujita, K. Ozaki, and N. Uchida, "Dynamic analysis and control for resonant currents in a zone-control induction heating system," *IEEE Trans. Power Electron.*, vol. 28, no. 3, pp. 1297–1307, Mar. 2013.

[28] K. L. Nguyen, O. Pateau, S. Caux, P. Maussion, and J. Egalon, "Robustness of a resonant controller for a multiphase induction heating system," *IEEE Trans. Ind. Appl.*, vol. 51, no. 1, pp. 73–81, Jan./Feb. 2014.

[29] J. Egalon, S. Caux, P. Maussion, M. Souley, and O. Pateau, "Multiphase system for metal disc induction heating: Modeling and RMS current control," *IEEE Trans. Ind. Appl.*, vol. 48, no. 5, pp. 1692–1699, Sep. 2012.

[30] J. M. Burdío, F. Monterde, J. R. Garcia, L. A. Barragan, and A. Martinez, "A two-output series-resonant inverter for induction-heating cooking appliances," *IEEE Trans. Power Electron.*, vol. 20, no. 4, pp. 815–822, Jul. 2005.

[31] H. Sarnago, J. M. Burdío, and Ó. Lucía, "High-performance and cost-effective ZCS matrix resonant inverter for total active surface induction heating appliances," *IEEE Trans. Power Electron.*, vol. 34, no. 1, pp. 117–125, Jan. 2019.

[32] H. Sarnago, Ó. Lucía, A. Mediano, and J. M. Burdío, "Analytical model of the half-bridge series resonant inverter for improved power conversion efficiency and performance," *IEEE Trans. Power Electron.*, vol. 30, no. 8, pp. 4128–4143, Aug. 2015.

[33] H. Sarnago, Ó. Lucía, and J. M. Burdío, "A versatile resonant tank identification methodology for induction heating systems," *IEEE Trans. Power Electron.*, vol. 33, no. 3, pp. 1897–1901, Mar. 2018.

HÉCTOR SARNAGO (S'09–M'15–SM'19) received the M.Sc. degree in electrical engineering and the Ph.D. degree in power electronics from the University of Zaragoza, Spain, in 2010 and 2013, respectively. He is currently a Senior Postdoctoral Researcher with the Department of Electronic Engineering and Communications, University of Zaragoza. His main research interests include resonant converters and digital control for induction heating applications.

Dr. Sarnago is a member of the Aragon Institute for Engineering Research (I3A).

PABLO GUILLÉN (S'19) received the M.Sc. degree in industrial engineering from the University of Zaragoza, Zaragoza, Spain, in 2017. In 2017, he held a research internship with the Bosch and Siemens Home Appliances Group. He is currently pursuing the Ph.D. degree with the Department of Electronic Engineering and Communications, University of Zaragoza. His main research interests include resonant power converters and digital control applied to induction heating.

Mr. Guillén is a member of the Aragon Institute for Engineering Research (I3A).

JOSÉ M. BURDÍO (M'97–SM'12) received the M.Sc. and Ph.D. degrees in electrical engineering from the University of Zaragoza, Zaragoza, Spain, in 1991 and 1995, respectively.

He has been with the Department of Electronic Engineering and Communications, University of Zaragoza, where he is currently a Professor, the Head of the Group of Power Electronics and Microelectronics, and the Director of the BSH Power Electronics Laboratory, University of Zaragoza. In 2000, he was a Visiting Professor with the Center for Power Electronics Systems, Virginia Tech. He is the author of more than 80 international journal articles and over 200 articles in conference proceedings and the holder of more than 60 international patents. His main research interests include modeling of switching converters and resonant power conversion for induction heating and biomedical applications.

Dr. Burdío is a Senior Member of the Power Electronics and Industrial Electronics Societies. He is also a member of the Aragon Institute for Engineering Research.

OSCAR LUCIA (S'04–M'11–SM'14) received the M.Sc. and Ph.D. degrees (Hons.) in electrical engineering from the University of Zaragoza, Spain, in 2006 and 2010, respectively.

From 2006 and 2007, he held a research internship at the Bosch and Siemens Home Appliances Group. Since 2008, he has been with the Department of Electronic Engineering and Communications, University of Zaragoza, where he is currently an Associate Professor. From 2009 to 2012, he was a Visiting Scholar with the Center of Power Electronics Systems (CPES), Virginia Tech. His main research interests include resonant power conversion, wide-bandgap devices, and digital control, mainly applied to contactless energy transfer, induction heating, electric vehicles, and biomedical applications. In these topics, he has published more than 65 international journal articles and 145 conference papers, and he has filed more than 30 patents.

Dr. Lucía is an active member of the Power Electronics (PELS) and Industrial Electronics (IES) societies. He is a member of the Aragon Institute for Engineering Research (I3A). He was a Guest Associate Editor of the IEEE TRANSACTIONS ON INDUSTRIAL ELECTRONICS and the IEEE JOURNAL OF EMERGING AND SELECTED TOPICS IN POWER ELECTRONICS, in 2013 and 2015, respectively. He is currently an Associate Editor of the IEEE TRANSACTIONS ON INDUSTRIAL ELECTRONICS, IEEE OPEN JOURNAL OF INDUSTRIAL ELECTRONICS, and IEEE TRANSACTIONS ON POWER ELECTRONICS.